Tech Science Press

A New Finite Element Model with Manufactured Error for Additive Manufacturing

Zhaohui Xia[1,2], Zhihao He[2], Qifu Wang[1] and Yingjun Wang[2,*]

[1]National Enterprise Information Software Engineering Research Center, School of Mechanical Science and Engineering, Huazhong University of Science and Technology, Wuhan, 430074, China
[2]National Engineering Research Center of Novel Equipment for Polymer Processing, The Key Laboratory of Polymer Processing Engineering of the Ministry of Education (South China University of Technology), Guangdong Provincial Key Laboratory of Technique and Equipment for Macromolecular Advanced Manufacturing, South China University of Technology, Guangzhou, 510641, China
*Corresponding Author: Yingjun Wang. Email: wangyj84@scut.edu.cn
Received: 27 February 2020; Accepted: 07 April 2020

Abstract: Additive manufacturing (AM), adding materials layer by layer, can be used to produce objects of almost any shape or geometry. However, AM techniques cannot accurately build parts with large overhangs, especially for the large features close to horizontal, hanging over the void. The overhangs will make the manufactured model deviate from the design model, which will result in the performance of the manufactured model that cannot satisfy the design requirements. In this paper, we will propose a new finite element (FE) analysis model that includes the manufacturing errors by mimicking the AM layer by layer construction process. In such FE model, an overhang coefficient is introduced to each FE, which is defined by the support elements in the lower layer. By mimicking the AM process from the bottom layer to the top layer, all the FE properties are updated based on their overhang coefficients, which makes the computational model be able to predict the manufactured model with manufacturing errors. The proposed model can be used to predict the performance of the AM objects in the design stage, which will help the designers to improve their design by the simulation results.

Keywords: Additive manufacturing; manufacturing error; finite element analysis; overhangs; 3D printing

1 Introduction

Additive manufacturing (AM), which is known as three-dimensional (3D) printing [1,2], is a process of building objects by adding layer-upon-layer of materials. AM technologies have been developed rapidly in the past few years [1,2–4], which continues growing owing to the versatility and low cost for rapid prototyping and manufacturing applications [5]. AM technologies provide larger freedom for design compared with the existing subtractive manufacturing methods [6–8], which can produce almost any shape and geometry.

The process of AM slices the CAD model to 2D contour with a user-defined slice thickness in each level along the building axis and begins from the base 2D contour [9]. This stacking way will raise the error of the staircase effect [10], which decreases the layers to finish building the AM part. The building part accuracy is one of the key constraints in AM, which might be influenced by slice thickness, part build orientation, thermal errors, support structures and overhangs [11–16].

However, there are still some design limitations in additive manufacturing, which is widely featured by diverse processes. e.g., precisely building large overhangs, especially those hangs close to horizontal or over the void region [17–21]. The slope of the overhang θ should be limited to a maximum angle with respect to the build direction, it is a self-supporting part when the angle meets the criterion in the given print orientation [22] as shown in Fig. 1. The pivotal angle for metal is typically 45°, if a part in its intended build direction includes regions with overhang angles greater than the pivotal angle, it is not a self-supporting part, which requires support structures in the build process and needs to remove the support materials. This will increase material, printing and post-processing costs [23–25]. The overhang facing down the base plate surface determines the degree of overhanging, while a surface will be overhanging when its degree lower than the threshold angle [22,25,26]. The allowable overhang angle of plastics is lower than the metal overhang angle [25]. The manufactured model might be derailed from the original design model by the overhanging surfaces, resulting in that the performance of the manufacturing model cannot meet the design requirements [21]. This manufacturing error leads to the difference between the original design model and manufactured model, and generates the difference of the mechanical performance between these models, which cannot be predicted in advance that reducing the design efficiency.
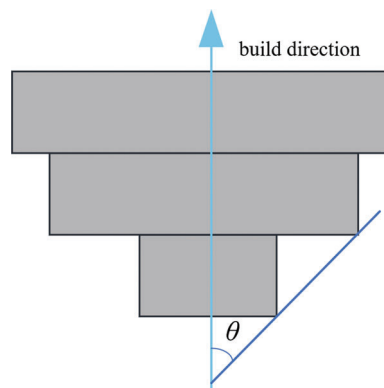

Figure 1: Illustration of the overhang angle

One of the approaches to address this problem is adopting support structures in the manufacturing processes [5,21,27–29]. However, these support structures will lead to increasing the building time and material cost, and removing support structures especially from the internal channels is also a difficult task [18]. Therefore, a new finite element (FE) analysis model is proposed in this paper to predict the final manufacturing geometric model and mechanical performance of the manufactured model.

So far, there are several researchers working on optimizing the generation of the support structures and find the more economical structures [12,14,17,22,25,30]. But few studies addressed the overhang accuracy to accurately predict the manufactured model with manufacturing errors and staircase effect caused by the offset between the printed layers before printing [17]. But the overhangs and staircase effects will make the manufactured model be deviated from the design model and cannot meet the design requirements.

To address this problem, a new finite element (FE) model that includes the manufacturing errors and staircase effects by mimicking the AM layer by layer construction process is proposed in this paper. By

mimicking the AM process from the bottom layer to the top layer, all the FE properties are updated based on their overhang coefficients, which makes the computational model can accurately predict the manufactured model with manufacturing errors. The proposed model can be used to predict the performance of the AM objects in the design stage, which will help the designers to improve their design by the simulation results.

The outline of the remainder of this paper is structured as follows: Section 2 briefly recapitulates the basic theory of the AM FE model. In Section 3, we propose the density updating strategy for each element in the background mesh. Several examples are used to validate the proposed updating algorithm and mechanics experiment to demonstrate the advantages of the proposed approach in Section 4. Finally, a brief summary is given in Section 5.

2 AM Finite Element Model

AM processes firstly extract the information from a computer-aided design (CAD) file [31], then convert to an approximated model based on triangles and sliced layers to be printed. In this section, a new FE model with the ability to predict manufacturing errors and the staircase effect of the AM objects is presented.

2.1 Background Mesh

The 3D objects for AM processes are generated from CAD models, which only carry boundary information (B-rep model) [32,33] without an appropriate mesh for finite element analysis. In this work, a voxel-based approach [34] for controlling the size of the domain is introduced to generate hexahedron meshes (including voxels). These meshes can be used as a background mesh to approximate the domain of the printing models via the spatial hashing calculation in the axis-aligned bounding boxes (AABBs) [35] for this AM model as shown in Fig. 2.
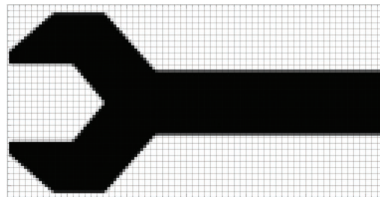

Figure 2: CAD model with the background mesh of the AM object

The domain of the CAD model is fully immersed in this background mesh with voxels, and the enclosed boundary curve of the model can be approximated as a polygon. Usually, the geometry of the additive manufacturing (AM) model is arbitrary. By using the point-in-polygon (PIP) algorithm [36], the hexahedron element (including multiple voxels) of the background mesh inside the arbitrary domain can be classified into three types as shown in Fig. 1: solid element, void element, and trimmed element. A trimmed element has two parts: retained part and removed part.

2.2 The Density of Each Hexahedron Element

If the element e in the background mesh is totally covered by the AM geometric model, the element is treated as a solid element and its relative ideal density τ_e is set to 1. If the element e is totally outside the AM geometric model, it is a void element. The element e partially covered by the AM geometric model is a trimmed element. To avoid any singularities, "ersatz material" approach [37] is adopted herein. In this method, a weak material with a small elastic modulus E_v will be adopted to fill the void element. E_v is usually less than 0.001 E_s that represents the elastic modulus of the solid material. Taking a 2D example, to obtain the density of the trimmed element e, the element will be subdivided into multiple voxels as shown in Fig. 3.
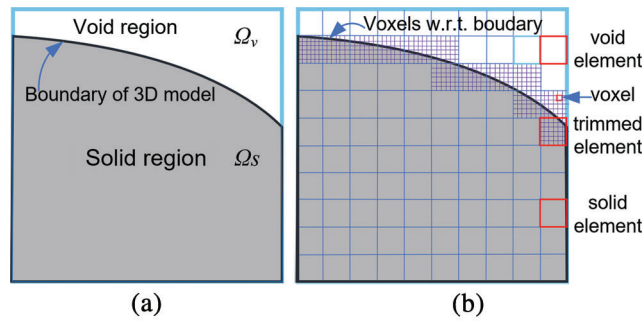
Figure 3: Subdivision of a trimmed element. (a) An element with the boundary (b) Subdivision with voxels of an element

The density τ_e of the trimmed element $e_{i,\,j,\,k}$ can be calculated by:

$$\tau_e = \frac{E_v \sum\limits_{p=1}^{P_e} p + E_s \sum\limits_{q=1}^{Q_e} q}{E_s \sum\limits_{n=1}^{N_e} n} \quad (N_e = P_e + Q_e), \tag{1}$$

where i, j and k denote the vertical (X), horizontal (Y) and depth (Z) location of the element, N_e represents the total number of voxels in one trimmed element, which is a specific value once the mesh is generated, P_e and Q_e are the numbers of voxels in the weak and solid material domains of this element. The different trimmed elements have a different number of solid material voxels, while the filling relative density τ_e will be in a range from 0 to 1. In this paper, the density of the 3D elements can be obtained from the extension of 2D elements. Herein we will use horizontal and vertical locations to describe the updating algorithm for simplicity the description in the following. For element $e_{i,j}$ to be printable, it should be sufficiently supported by its supporting area consisting of the elements below $e_{i,j}$ and the neighbors of $e_{i,j}$ as in Fig. 4. This is motivated by the critical self-supporting overhang angle and inspired by the additive manufacturing filter proposed in [22,25]. We assumed that the fused material can flow, and the density of $e_{i,j}$ would not drop directly without any resistance when its below element cannot support it, since the below might not be completely overhanging. The dropped material could not be completely embedded underneath, and they might spread around. The final print density $\rho_{e_{i,j}}$, which can be expressed by Eq. (2). The density of this element and the density of the entire support area as shown in Fig. 4 are
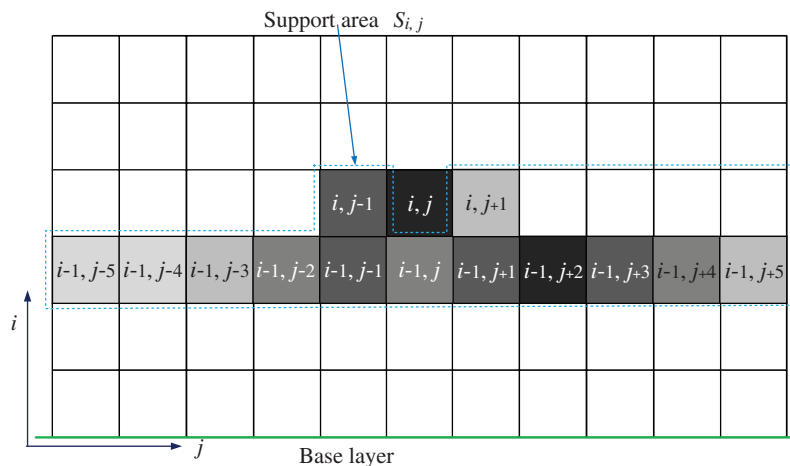

Figure 4: Definition of supporting area $S_{i,j}$ for element $e_{i,j}$

$$\rho_{e_{i,j}} = \Omega(\tau_{e_{i,j}}, \ \Phi_{e_{i,j}})$$
$$\Phi_{e_{i,j}} = \{\tau_{e_{\eta,\xi}} | e_{\eta,\xi} \in S_{i,j}\}$$

(2)

where $\Phi_{e_{i,j}}$ is a set of density of the elements in the support area of $e_{i,j}$. Ω represents the calculation function based on the layer-based updating algorithm described in detail in Section 3. $E_{\eta, \xi}$ denotes the element locating at η in x-axis and ξ in the y-axis, $S_{i,j}$ represents the set of elements in the support area of element $e_{i,j}$.

2.3 FEM Calculation

The problem presented herein is elastostatics, and the two-dimensional plane-stress problem is taken as an example to illustrate the calculation formulation. From the theory of continuum mechanics, the formulation of an elastic finite element method beginning with the equilibrium equations can be expressed as [38]:

$$\frac{\partial \sigma_x}{\partial x} + \frac{\partial \tau_{xy}}{\partial y} + f_x = 0$$
$$\frac{\partial \tau_{xy}}{\partial x} + \frac{\partial \sigma_y}{\partial y} + f_y = 0$$

(3)

where i,j are the index notations, σ and τ represent normal and shear stress, respectively. f_x and f_y are body force components in x and y direction, respectively. The in-plane stress field forms a tensor defined by three independent components: σ_{xx}, σ_{yy} and τ_{xy}, and they can be expressed as:

$$
\begin{Bmatrix} \sigma_{xx} \\ \sigma_{yy} \\ \tau_{xy} \end{Bmatrix} = \begin{bmatrix} D_{11} & D_{12} & 0 \\ D_{21} & D_{22} & 0 \\ 0 & 0 & D_{33} \end{bmatrix} \begin{Bmatrix} \varepsilon_{xx} \\ \varepsilon_{yy} \\ \varepsilon_{xy} \end{Bmatrix}
$$
$$
= \frac{E}{1-v^2} \begin{bmatrix} 1 & v & 0 \\ v & 1 & 0 \\ 0 & 0 & \frac{1-v}{2} \end{bmatrix} \begin{Bmatrix} \varepsilon_{xx} \\ \varepsilon_{yy} \\ \varepsilon_{xy} \end{Bmatrix},
$$
$$
= D \begin{Bmatrix} \varepsilon_{xx} \\ \varepsilon_{yy} \\ \varepsilon_{xy} \end{Bmatrix}
$$

(4)

where D is the 3 × 3 stress-strain matrix, E represents elastic modulus, v is Poisson's ratio. ε, γ represents normal strain and shear strain, which can be indicated as:

$$
\varepsilon = \begin{bmatrix} \frac{\partial N_1}{\partial x} & 0 & \frac{\partial N_2}{\partial x} & 0 & \cdots & \frac{\partial N_n}{\partial x} & 0 \\ 0 & \frac{\partial N_1}{\partial y} & 0 & \frac{\partial N_2}{\partial y} & \cdots & 0 & \frac{\partial N_n}{\partial y} \\ \frac{\partial N_1}{\partial y} & \frac{\partial N_1}{\partial x} & \frac{\partial N_2}{\partial y} & \frac{\partial N_2}{\partial x} & \cdots & \frac{\partial N_n}{\partial y} & \frac{\partial N_n}{\partial x} \end{bmatrix} u
$$
$$
= Bu
$$

(5)

$$u = Nu_e$$

$$\varepsilon_{xx} = \frac{\partial u_x}{\partial x}; \quad \varepsilon_{yy} = \frac{\partial u_y}{\partial y}; \quad \varepsilon_{xy} = \frac{1}{2}\left(\frac{\partial u_x}{\partial y} + \frac{\partial u_y}{\partial x}\right);$$

where B is the strain-displacement matrix, u is the nodal displacement, N_i is the element shape function. Based on the principle of minimum potential energy [39], the potential energy Π_e of each element for the plane stress problem is given by:

$$
\begin{aligned}
\Pi_e &= \frac{1}{2}\int_{\Omega_e}\sigma^T\varepsilon d\Omega_e - \int_{\Omega_e}u^TXd\Omega_e - \int_{\Gamma_e}u^T\widehat{t}d\Gamma_e\\
&\approx \frac{1}{2}(u_e)^T\left(\int_{\Omega_e}B^TDBd\Omega_e\right)u - (u_e)^T\left(\int_\Omega N^TXd\Omega_e + \int_{\Gamma_e}N^T\widehat{t}d\Gamma_e\right),\\
&= \frac{1}{2}(u_e)^TK_e(u_e) - (u_e)^Tf
\end{aligned}
\tag{6}
$$

where Ω_e and Γ_e represent the domain and boundary of element e. u_e are the node displacement vector of element e, $\mathbf{X}$ is the body force, K_e is the stiffness of element e, N is the shape function, $\widehat{t}$ represents surface tractions, f is the element nodal load vector. From the principle of minimum potential energy, the equilibrium equations can be expressed as:

$$
\frac{\partial\Pi_e}{\partial u_e} = K_eu_e - f = 0,
\tag{7}
$$

For the whole elements, the equilibrium equation in which nodal displacements u are the unknowns can be written as:

$$
Ku = f,
\tag{8}
$$

where K is the stiffness matrix, u is the nodal displacement vector and f is the element nodal load vector, while K is assembled by the element stiffness matrix K_e. From Eq. (6), the element stiffness matrix can be expressed as [40]:

$$
\begin{aligned}
K_e &= \int_{\Omega_e}B^TDBd\Omega_e\\
&= \int_{\Omega_e}B^TDB|J_1|d\Omega_e
\end{aligned}
\tag{9}
$$

in which B is the strain-displacement matrix and D is the stress-strain matrix. Ω_e represents the domain of the element. $\tilde{\Omega}_e$ is the integration domain in the integration of parametric space. To evaluate the performance of the proposed FEM model with manufacturing errors, the element stiffness matrix can be described with print density $\rho_{e_{i,j}}$ as:

$$
\begin{aligned}
K'_e &= \int_{\Omega_e}B^TDB|J_1|\rho(\Phi)d\Omega_e\\
&= K_e \cdot \rho_e
\end{aligned}
\tag{10}
$$

where K_e represents the stiffness matrix of a full-solid element, and it can be expressed discretely as

$$
\begin{aligned}
K_e &= \int_{S_e}B^TDBdS_e\\
&= \sum_{i=1}^n w_iB_i^TD_iB_i
\end{aligned}
\tag{11}
$$

in which B_i is the strain-displacement matrix and D_i is the stress-strain matrix related to the ith quadrature point. S_e is the domain of the element.

3 Update of FE Properties

For an element $e_{i,j}$ to be printable, it should be adequately supported by the elements belonging to $S_{i,j}$. The elements supported by the base layer ($i = 1$) can be printed. For the above layers, the print density $\rho_{e_{i,j}}$ of element $e_{i,j}$ cannot be greater than the threshold density $\delta_{e_{i,j}}$ (if greater, the materials will drop into its supported area, and finally up to a balance to be equal) supported by the elements in $S_{i,j}$. The support area consists of a set of neighbor elements S_2, a set of below elements S_1 ($S_1 + S_2 = S_{i,j}$) as shown in Fig. 3. In this work, the threshold density $\delta_{e_{i,j}}$ of element $e_{i,j}$ is approximately opted as:

$$
\delta_{e_{i,j}} = \varphi_1 \times \omega_b + \varphi_2 \times \omega_s \quad (\omega_b + \omega_s = 1),
$$

$$
\varphi_1 = -\frac{1}{\mu} \log \left(\sum_{n=1}^{N} e^{-\mu \times \tau_{e_n}} \times \omega_n \right) \quad (e_n \in S_1),
$$

$$
\varphi_2 = \sum_{m=1}^{M} \tau_{e_m} \times \omega_m \quad (e_m \in S_2),
$$

$$
\delta_{e_{i,j}} = -\frac{1}{\mu} \log (\sum_{n=1}^{N} e^{-\mu \times \tau_{e_n}} \times \omega_n) \times \omega_b + (\sum_{m=1}^{M} \tau_{e_m} \times \omega_m) \times \omega_s
$$

(12)

$$
\sum_{n=1}^{N} \omega_n = 1, \quad \sum_{m=1}^{M} \omega_m = 1
$$

(13)

where φ_1 calculates a suitable approximate threshold density from the elements in the layer below of the supporting area, which approaches $\varphi_1 \rightarrow \min (\tau_{e_n})$ as $\rho \rightarrow +\infty$. μ is overhang coefficient for calculation controlling the smoothness of the approximations, ω_b and ω_s ($\omega_b + \omega_s = 1$) are the weights in the below layer and the same layer (i.e., neighbor) of element $e_{i,j}$ separately, while ω_b should be greater than ω_s since it has a higher opportunity to drop into the below layer than in the same layer (they are set to 0.8 and 0.2 in the examples of this paper). ω_n and ω_m represents the different weights of each element inside the support area of element $e_{i,j}$. ω_n is calculated as:

$$
\omega_n' = e^{\frac{-x_n}{\sqrt{(x_n - d)^2 + \varepsilon}}}
$$

$$
\omega_n = \frac{\omega_n'}{\sum_{n=1}^{N} \omega_n'}
$$

(14)

where N is the total number of elements S_1 inside the support area, d is the threshold distance between the element e_n and $e_{i,j}$ while x_n is the distance between e_n and $e_{i,j}$. ε is set to 10^{-6} to avoid infinity herein. ω_m can be expressed as:

$$
\omega_m' = \sqrt{\frac{d - x_m}{d}}
$$

$$
\omega_m = \frac{\omega_m'}{\sum_{m=1}^{M} \omega_m'}
$$

(15)

In which, M is the total number of elements S_2 inside the support area, d is the threshold distance between the element e_m and $e_{i,j}$. The weight distribution of ω_n and ω_m is shown in Fig. 5.
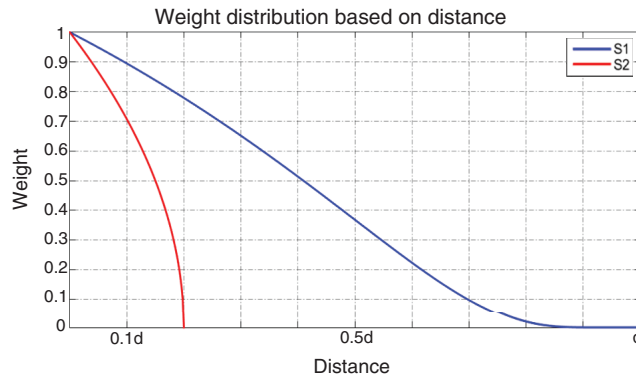
Figure 5: Weight distribution based on different distance

If the printed density $\rho_{e_{i,j}}$ of element $e_{i,j}$ is greater than $\delta_{ei,j}$, we assume that a part of FE properties (material/density) in the element $e_{i,j}$ will drop into its support area, which means the print density of $e_{i,j}$ and the elements in its support area should be updated. This paper proposes an updating algorithm to revise the density of each element. Updating the density of the printable elements should be from the second layer to the top layer ($i = nely$) as shown in Fig. 6, since the base layer ($i = 1$) can be printed directly. Meanwhile, the updating algorithm will be recursive since each element that drops material influences the element density in the below layers.
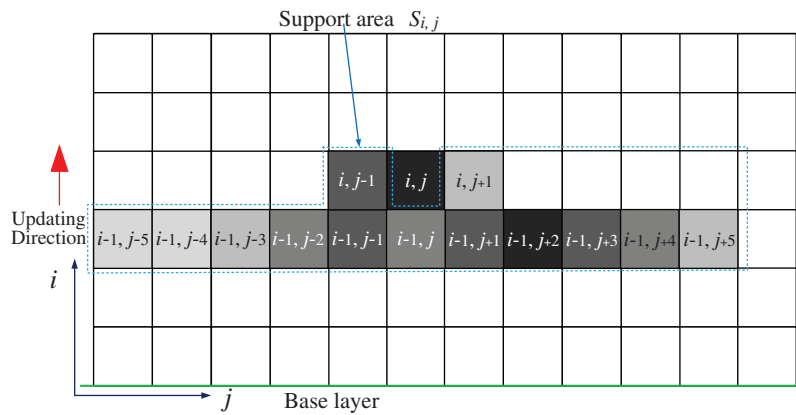
Figure 6: Updating direction compared with the base layer

When the density of the element $e_{i,j}$ drops into its support area, the dropping density Δ can be expressed as:

$$\Delta_e = \frac{\tau_e - \delta_e}{N}$$
$$\rho'_e = \tau_e - \Delta_e$$

(16)

where N is the iteration number of dropping procedure (minimum is 2) in each loop, ρ'_e represents the temporary density during the calculation procedure. To accurately describe the dropping procedure. The updated FE density of each element can be expressed as:

$$\rho'_n = \tau_n + \theta \times \omega_n \times \omega_b \quad \{e_n \in S_1\}$$
$$\rho'_m = \tau_m + \theta \times \omega_m \times \omega_s \quad \{e_m \in S_2\}$$

(17)

The updating algorithm of FE properties can be briefly described in Algorithm 1. The function in the algorithm update Density is called recursively since the FE properties of its influenced element should be updated once it is revised by the updating algorithm.

Algorithm 1: Recursion function of updating algorithm

updateDensity (*i, j, nelx, nely, ρ, lev, maxlev*): updating the density of element $e_{i,j}$ and its supporting elements

i, j: the layer of element *e* in the vertical direction and horizontal direction
nely, nelx: the number of elements in the vertical and horizontal direction
maxlev: the maximum of dropping layer   *lev*: the current updating layer
ρ: the print density matrix of the entire elements
1: if *i* > *nely*-1 return;
2: if *lev* > *maxDropLayer* return;
3: *lev* ← *lev*+1
4: for *n* ∈ *s*1 do
5: $\omega_n \Leftarrow \text{norm}(e^{-x_n/((x_n-d)^2+\varepsilon)})$
6: $\varphi_n + = e^{-\mu \times \rho_n} \times \omega_n$
7: end
8: $\varphi_n = {-1}/{\mu} \log(\varphi_n)$
9: for *m* ∈ S_2 do
10: $\omega_m \Leftarrow \text{norm}(\sqrt{(d-x_m)/d})$
11: $\varphi_m + = \rho_m \times \omega_m$
12: end
13: $\delta_{i,j} \Leftarrow \varphi_m \times \omega_b + \varphi_n \times \omega_s$
14: if $\delta_{i,j} > \tau_{i,j} \; \rho_{i,j} \Leftarrow \tau_{i,j}$
15: elseif $\delta_{i,j} > 0$
16:    move $\Leftarrow (\tau_{i,j} - \delta_{i,j})$/iternum
17:    $\rho_{i,j}=\tau_{i,j}$−move
18:    for *n* ∈ S_1 do
19:       $\rho'_n \Leftarrow \tau_{i,j}$+move×$\omega_n$×$\omega_b$
20:       *ii, jj* ← S_{1n} // *ii* and *jj* indicate element position in vertical and horizontal direction
21:       updateDensity(*ii, jj, nelx, nely, ρ, lev*);
22:    endfor
23:    for *m* ∈ S_2 do
24:       $\rho'_m \Leftarrow \tau_{i,j}$+move×$\omega_m$×$\omega_s$
25:       *ii, jj* ← S_{2m}
26:    updateDensity(*ii, jj, nelx, nely, ρ, lev*);
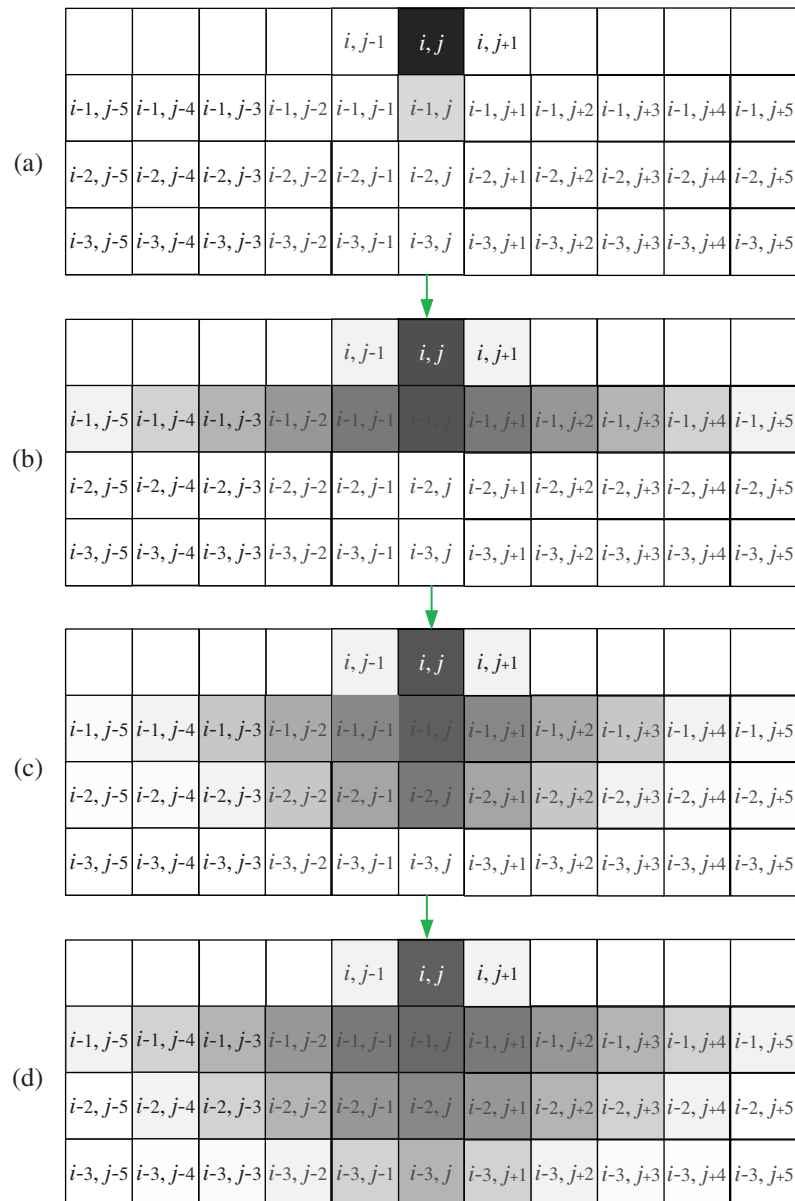27:   endfor
28: endif

Figure 7: Updating procedures

The updating procedure can be shown in detail in Fig. 7. For each element to be printable, it should be supported, otherwise, some of the materials would drop to its supporting area. Some materials of the elements in the supporting area would drop to their supporting area as well. We assumed that the maximum dropping layer would be a different value for different additive manufacturing process:

- Updating density after one layer dropping: Figs. 7a and 7b shows the initial density distribution of one element, from the calculation, $\tau_{i,j}$ is greater than $\varphi_{i,j}$, then some FE densities will drop into their support area, which makes the elements inside its support area change the density.
- Updating density after several layers' dropping: Once the whole influenced elements are updated completely, the updating procedure will move to the next element updating procedure with recursion due to the changed density of elements as shown in Fig. 7c.

- Updating density after the dropping stops: When the whole updating procedure is done, the FE properties might obtain a relatively stable status, which means that each element is successfully supported by its supported area as shown in Fig. 7d.

4 Numerical Examples and Experiment Results

To illustrate the functionality and characteristics of the proposed method, two models (spanner and dog-bone-shaped specimen) are used to validate the algorithm with the FDM process, while the deposition path pattern is not in the consideration of the experiments. According to the features of FDM, the default parameters of the for the two cases are listed as: $\omega_b = 0.7$, $\omega_s = 0.3$, $d = 5.0$, $\mu = -200$, $\varepsilon = 0.00001$, $E_s = 10000$, Poisson's ratio $\gamma = 0.3$. The proposed method also can be extended to other methods, and these parameters and the assumption condition should be adjusted. The 3D printer used to manufacture the models is Zmorph 2.0 SX (Zmorph, Wroclaw, Poland).

(1) Case 1: Spanner model

To validate the manufactured error, an example with spanner model is adopted with two type manufacturing direction: (1) Upright printing: using the bottom face as the base layer shown in Fig. 8a; (2) Laydown printing: using the face having the maximum cross-sectional area as the base layer shown in Fig. 8b, which will reduce the manufacturing error at the maximum. Both of the two ways are applied to the same boundary condition (displacement constraints and load) for FEM analysis as shown in Fig. 8c.
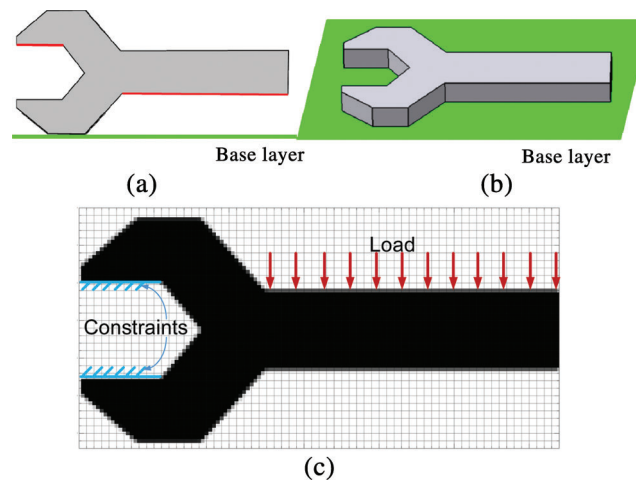

Figure 8: Spanner model with background mesh. (a) Upright printing (b) Case 2: Laydown printing and (c) Boundary conditions for FEM analysis

For laydown printing, the whole elements will be supported by their support area. The final density distribution after updating density distribution is nearly the original one as shown in Fig. 9a. For upright printing, the density of the whole elements will be updated based on the algorithm in Section 3, since the elements of the AM model in the right bottom area cannot be supported by their support areas. All the trimmed elements are near the boundary of the 3D printing model, the ideal density can be obtained based on the voxel number in each element. Due to the updating algorithm, a few materials of some elements (element properties) will drop into their supported area, which leads to new density distribution. The new density distribution is a little different from the original one treating as manufacturing error marked inside blue line as shown in Fig. 9b, which is similar to the manufacturing result (the dropping
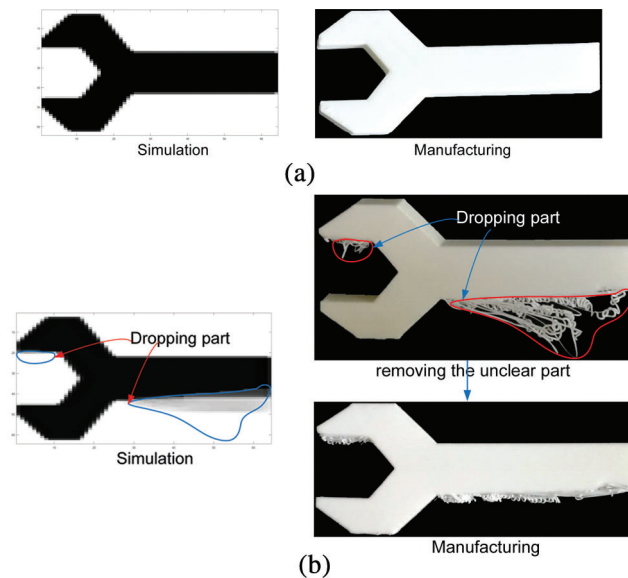
Figure 9: Comparison between laydown and upright printing. (a) Results of simulation and manufacturing for laydown printing and (b) Results of simulation and manufacturing for upright printing

parts are marked inside red line). Therefore, the updating algorithm has the potential ability to predict the manufactured model.

To compare the mechanical analysis between the simulated manufactured results, FEM analysis and mechanical experiments are employed. The results are listed in Tabs. 1 and 2, which shows that the distribution is similar but different maximum displacement and Von Mises value.

To compare the relative error between the model with manufacturing error and the original model, the error is defined as:

$$\varepsilon = \frac{|D_m - D_o|}{D_o} \tag{18}$$

in which D_m represents the maximum total displacement or Von Mises stress of the FEM model with a manufacturing error, while D_o indicates the maximum total displacement or Von Mises stress of the original model, ε is the relative error between these two models. The FEM model with the manufacturing error can be generated as shown in Fig. 10. The relative error of total displacement herein is about 8.9% (about 4.8% when using ANSYS), while the relative error of Von-Mises stress is about 10.9% (about 4.0% when using ANSYS).

To compare the relative error between the experiments and the simulation, 3 groups of upright and laydown printing are used for tensile and 3-point bending testing as shown in Fig. 11. The maximum tensile and bending stress for the laydown printing are 42.6 Mpa and 59.6 MPa, respectively, while for upright printing, they are 37.5 MPa and 53.6 MPa. The relative error of tensile and bending stress between the upright and laydown printing is about 12.0% and 10.0%, respectively. The mechanical experiments show that the simulation result is close to the experiment, which shows the proposed updating algorithm can predict the performance of the AM model with the manufacturing error.

(2) Case 2: Dog-bone-shaped model

Here is another example with a dog-bone-shaped model adopting two types of manufacturing direction as Case 1 shown in Figs. 12 and 13.

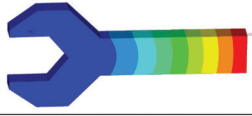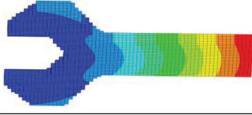**Table 1:** Comparison of the displacement for the different types
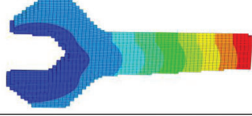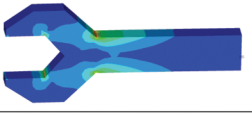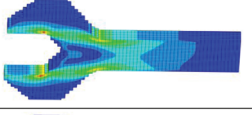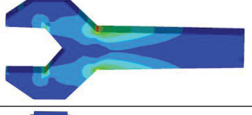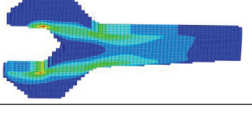
Types	Displacement Min — Max	Relative Error
		U–A/L–A ≈ 4.8% U–M/L–M ≈ 8.9%
Laydown-ANSYS (L-A)		Min=0 Max=0.756
Laydown-our model (L-M)		Min=0 Max=0.745
Upright-ANSYS (U-A)		Min=0 Max=0.792
Upright-our model (U-M)		Min=0 Max=0.811

Table 2: Comparison of the Von Mises stress for the different types

Types	Von Mises stress Min — Max	Relative Error
		U–A/L–A ≈ 4.0% U–M/L–M ≈ 12.1%
Laydown-ANSYS (L-A)		Min=0.014 Max=81.158
Laydown-our model (L-M)		Min=0.016 Max=79.863
Upright-ANSYS (U-A)		Min=0.019 Max=77.934
Upright-our model (U-M)		Min=0.016 Max=70.126

For laydown printing, the whole elements are supported by their support area while the density of the whole elements is updated for the upright printing case. Some materials of the middle elements drop into their supported area leading to new density distribution. The new density distribution of the simulation with manufacturing error marked inside the blue line as shown in Fig. 12 is a little different from the original one as shown in Fig. 13, which is similar to the manufacturing result. It shows that the updating algorithm can predict the manufactured model.
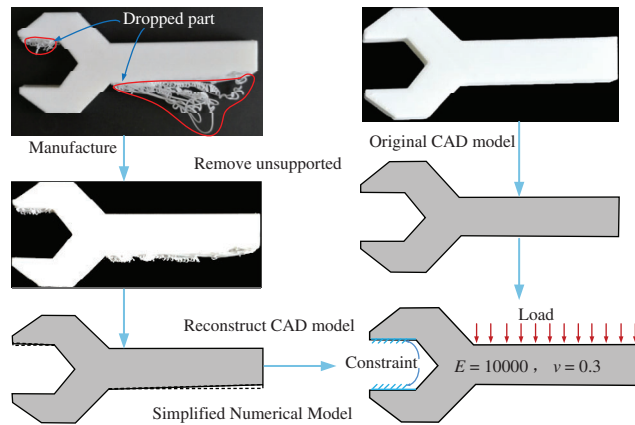
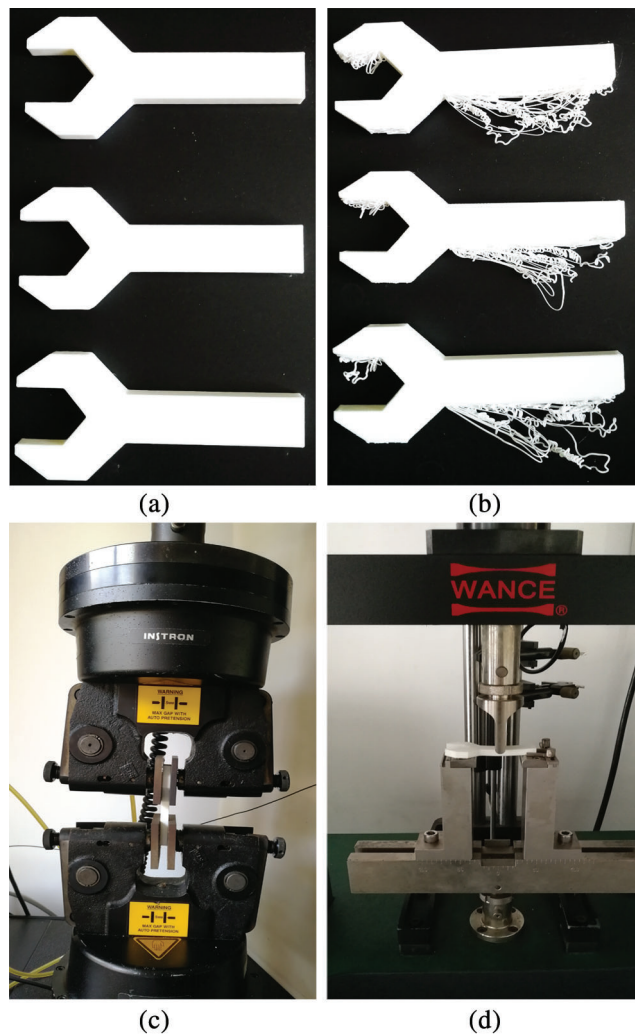**Figure 10:** Generating the numerical model with manufacturing error

Figure 11: Three groups for the experiment. (a) Laydown cases (b) Upright printing cases (c) Tensile testing and (d) 3-Point bending testing
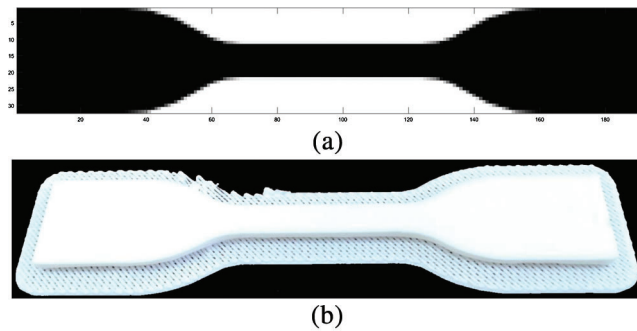
Figure 12: Laydown printing: no overhang. (a) AM geometric model without updating density and (b) AM model after manufacturing
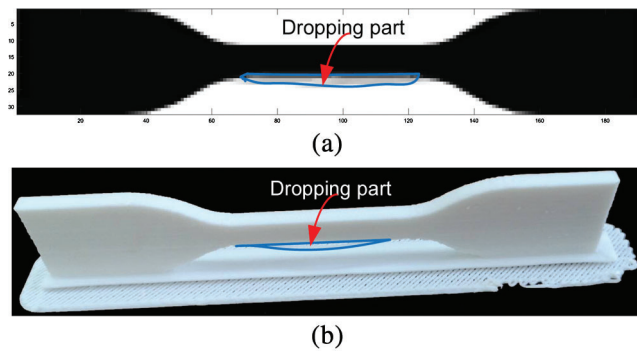

Figure 13: Upright printing: overhangs. (a) AM geometric model with updating density and (b) AM model after manufacturing

To compare the relative error between the experiments and the simulation, 5 groups of upright and laydown printing are used for tensile testing as shown in Fig. 14. From Fig. 14a, it can be found that the broken position is random since the middle part of the dog-bone-shaped specimens should be isostress, and any randomly slight manufacturing error may break the isostress status and results in the random broken position. However, due to error caused by the printing direction, all the broken positions locate at the ends of the middle part of dog-bone-shaped specimens, which further demonstrates that overhangs will influence the performance of the printed structures. Therefore, it is of importance to propose a method that can predict manufacturing error before manufacturing.
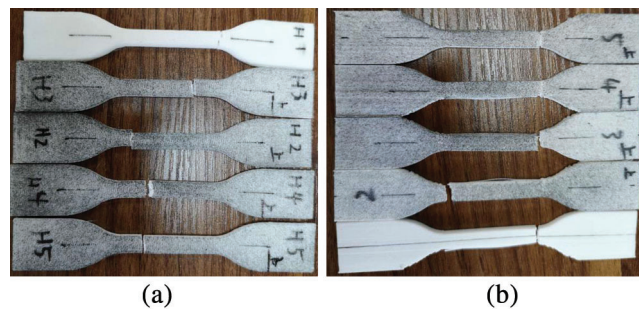

Figure 14: Five groups for the experiment. (a) Laydown printing tensile testing and (b) Upright printing tensile testing

5 Discussion/Conclusion

A new computational model including the manufacturing errors by mimicking the AM processes is presented. With this method, the density of each element is updated automatically layer by layer in the design stage, which can help designers predict the performance of the CAD model for AM processes.

Two AM model examples with numerical and experimental tests with two printing types are employed to validate the manufactured error. Based on the simulation and experimental results, the proposed model can approximately predict the final performance in the design stage.

Although the focus of the present paper is the FEM model with manufactured error is described in 2D contour with the same density in the z-axis, it can be extended to 3D problems (different density in the z-axis). Besides that, updating the algorithm is still being improved and may be different for different AM types, such as FDM (fused deposition modeling), SLM (selective laser melting), SLA (stereolithography appearance), etc., and the parameters in the threshold density calculation also need to be optimized.

Conflicts of Interest: The authors declare that they have no conflicts of interest to report regarding the present study.

References

1. Paolini, A., Kollmannsberger, S., Rank, E. (2019). Additive manufacturing in construction: a review on processes, applications, and digital planning methods. *Additive Manufacturing, 30,* 100894. DOI 10.1016/j.addma.2019.100894.

2. Culmone, C., Smit, G., Breedveld, P. (2019). Additive manufacturing of medical instruments: a state-of-the-art review. *Additive Manufacturing, 27,* 461–473. DOI 10.1016/j.addma.2019.03.015.

3. Tay, Y. W. D., Panda, B., Paul, S. C., Mohamed, N. A. N., Tan, M. J. et al. (2017). 3D printing trends in building and construction industry: a review. *Virtual and Physical Prototyping, 12(3),* 261–276. DOI 10.1080/17452759.2017.1326724.

4. Delgado Camacho, D., Clayton, P., O'Brien, W. J., Seepersad, C., Juenger, M. et al. (2018). Applications of additive manufacturing in the construction industry—a forward-looking review. *Automation in Construction, 89,* 110–119. DOI 10.1016/j.autcon.2017.12.031.

5. Wong, K. V., Hernandez, A. (2012). A review of additive manufacturing. *ISRN Mechanical Engineering, 2012(4),* 1–10. DOI 10.5402/2012/208760.

6. Parandoush, P., Lin, D. (2017). A review on additive manufacturing of polymer-fiber composites. *Composite Structures, 182,* 36–53. DOI 10.1016/j.compstruct.2017.08.088.

7. Saengchairat, N., Tran, T., Chua, C. K. (2017). A review: additive manufacturing for active electronic components. *Virtual and Physical Prototyping, 12(1),* 31–46. DOI 10.1080/17452759.2016.1253181.

8. Yan, W., Lin, S., Kafka, O. L., Lian, Y., Yu, C. et al. (2018). Data-driven multi-scale multi-physics models to derive process-structure-property relationships for additive manufacturing. *Computational Mechanics, 61(5),* 521–541. DOI 10.1007/s00466-018-1539-z.

9. Das, P., Chandran, R., Samant, R., Anand, S. (2015). Optimum part build orientation in additive manufacturing for minimizing part errors and support structures. *Procedia Manufacturing, 1,* 343–354. DOI 10.1016/j.promfg.2015.09.041.

10. Ghaffar, S. H., Corker, J., Fan, M. (2018). Additive manufacturing technology and its implementation in construction as an eco-innovative solution. *Automation in Construction, 93,* 1–11. DOI 10.1016/j.autcon.2018.05.005.

11. Kajima, Y., Takaichi, A., Nakamoto, T., Kimura, T., Kittikundecha, N. et al. (2018). Effect of adding support structures for overhanging part on fatigue strength in selective laser melting. *Journal of the Mechanical Behavior of Biomedical Materials, 78,* 1–9. DOI 10.1016/j.jmbbm.2017.11.009.

12. Jiang, J., Xu, X., Stringer, J. (2018). Support structures for additive manufacturing: a review. *Journal of Manufacturing and Materials Processing, 2(4),* 64. DOI 10.3390/jmmp2040064.

13. Cloots, M., Zumofen, L., Spierings, A. B., Kirchheim, A., Wegener, K. (2017). Approaches to minimize overhang angles of SLM parts. *Rapid Prototyping Journal, 23(2),* 362–369. DOI 10.1108/RPJ-05-2015-0061.

14. Langelaar, M. (2018). Combined optimization of part topology, support structure layout and build orientation for additive manufacturing. *Structural and Multidisciplinary Optimization, 57(5),* 1985–2004. DOI 10.1007/s00158-017-1877-z.

15. Fox, J. C., Moylan, S. P., Lane, B. M. (2016). Effect of process parameters on the surface roughness of overhanging structures in laser powder bed fusion additive manufacturing. *Procedia CIRP, 45,* 131–134. DOI 10.1016/j.procir.2016.02.347.

16. Wu, J., Wang, C. C. L., Zhang, X., Westermann, R. (2016). Self-supporting rhombic infill structures for additive manufacturing. *Computer-Aided Design, 80,* 32–42. DOI 10.1016/j.cad.2016.07.006.

17. Maidin, S., Mohamed, A. S., Akmal, S., Mohamed, S. B., Wong, J. H. U. (2018). Feasibility study of vacuum technology integrated fused deposition modeling to reduce staircase effect. *Journal of Fundamental and Applied Sciences, 10,* 633–645.

18. Badiru, A. B., Valencia, V. V., Liu, D. (2017). *Additive manufacturing handbook: product development for the defense industry.* CRC Press, USA.

19. Gao, W., Zhang, Y., Ramanujan, D., Ramani, K., Chen, Y. et al. (2015). The status, challenges, and future of additive manufacturing in engineering. *Computer-Aided Design, 69,* 65–89. DOI 10.1016/j.cad.2015.04.001.

20. Huang, Y., Leu, M. C., Mazumder, J., Donmez, A. (2015). Additive manufacturing: current state, future potential, gaps and needs, and recommendations. *Journal of Manufacturing Science and Engineering, 137(1),* 014001–014010. DOI 10.1115/1.4028725.

21. Bikas, H., Stavropoulos, P., Chryssolouris, G. (2016). Additive manufacturing methods and modelling approaches: a critical review. *International Journal of Advanced Manufacturing Technology, 83(1–4),* 389–405. DOI 10.1007/s00170-015-7576-2.

22. Langelaar, M. (2016). Topology optimization of 3D self-supporting structures for additive manufacturing. *Additive Manufacturing, 12,* 60–70. DOI 10.1016/j.addma.2016.06.010.

23. Wang, Y., Gao, J., Kang, Z. (2018). Level set-based topology optimization with overhang constraint: towards support-free additive manufacturing. *Computer Methods in Applied Mechanics and Engineering, 339,* 591–614. DOI 10.1016/j.cma.2018.04.040.

24. Lindemann, C., Jahnke, U., Moi, M., Koch, R. (2012). Analyzing product lifecycle costs for a better understanding of cost drivers in additive manufacturing. *23th Annual International Solid Freeform Fabrication Symposium—An Additive Manufacturing Conference*, Austin Texas USA, *6th-8th August,* 177–188.

25. Langelaar, M. (2017). An additive manufacturing filter for topology optimization of print-ready designs. *Structural and Multidisciplinary Optimization, 55(3),* 871–883. DOI 10.1007/s00158-016-1522-2.

26. Turner, B. N., Strong, R., Gold, S. A. (2014). A review of melt extrusion additive manufacturing processes: I. Process design and modeling. *Rapid Prototyping Journal, 20(3),* 192–204. DOI 10.1108/RPJ-01-2013-0012.

27. Gradl, P., Brandsmeier, W., Calvert, M., Greene, S., O'Neal, D. et al. (2017). Additive manufacturing overview: propulsion applications, design for and lessons learned. *NASA Technical Reports,* 1–39.

28. Costabile, G., Fera, M., Fruggiero, F., Lambiase, A., Pham, D. (2017). Cost models of additive manufacturing: a literature review. *International Journal of Industrial Engineering Computations, 8,* 263–283. DOI 10.5267/j.ijiec.2016.9.001.

29. Yan, J., Yan, W., Lin, S., Wagner, G. J. (2018). A fully coupled finite element formulation for liquid-solid-gas thermo-fluid flow with melting and solidification. *Computer Methods in Applied Mechanics and Engineering, 336,* 444–470. DOI 10.1016/j.cma.2018.03.017.

30. Garaigordobil, A., Ansola, R., Santamaría, J., Fernández de Bustos, I., (2018). A new overhang constraint for topology optimization of self-supporting structures in additive manufacturing. *Structural and Multidisciplinary Optimization, 58(5),* 2003–2017. DOI 10.1007/s00158-018-2010-7.

31. Boparai, K. S., Singh, R., Singh, H. (2016). Development of rapid tooling using fused deposition modeling: a review. *Rapid Prototyping Journal, 22(2),* 281–299. DOI 10.1108/RPJ-04-2014-0048.

32. Xia, Z., Wang, Q., Wang, Y., Yu, C. (2015). A CAD/CAE incorporate software framework using a unified representation architecture. *Advances in Engineering Software, 87,* 68–85. DOI 10.1016/j.advengsoft.2015.05.005.

33. Xia, Z., Wang, Q., Liu, Q., Wang, Y., Liu, J. et al. (2016). A novel approach for automatic reconstruction of boundary condition in structure analysis. *Advances in Engineering Software, 96,* 38–57. DOI 10.1016/j.advengsoft.2016.02.001.

34. Brackett, D., Ashcroft, I., Hague, R. (2011). Topology optimization for additive manufacturing. *Proceedings of the Solid Freeform Fabrication Symposium, 1,* 348–362.

35. Hastings, E. J., Mesit, J., Guha, R. K. (2005). Optimization of large-scale, real-time simulations by spatial hashing. *Proceedings of the 2005 Summer Computer Simulation Conference, 37(4),* 9–17, Cherry Hill, New Jersey, USA.

36. Deng, X., Wang, Y., Yan, J., Liu, T., Wang, S. (2015). Topology optimization of total femur structure: application of parameterized level set method under geometric constraints. *Journal of Mechanical Design, 138(1),* 1545. DOI 10.1115/1.4031803.

37. Wang, Y., Benson, D. J. (2016). Isogeometric analysis for parameterized LSM-based structural topology optimization. *Computational Mechanics, 57(1),* 19–35. DOI 10.1007/s00466-015-1219-1.

38. Owens, B. C. (2010). *Implementation of B-splines in a conventional finite element framework (Ph.D. Thesis).* Texas A & M University, USA.

39. Nikishkov, G. P. (2004). *Introduction to the finite element method (lecture notes).* University of Aizu, Japan.

40. Wang, Y., Benson, D. J., Nagy, A. P. (2015). A multi-patch nonsingular isogeometric boundary element method using trimmed elements. *Computational Mechanics, 56(1),* 1–19.